Optik 127 (2016) 2266–2270

Contents lists available at ScienceDirect

Optik

journal homepage: www.elsevier.de/ijleo

Structural, morphological, optical and electrical characterization of spray ultrasonic deposited SnS_2 thin film

I. Bouhaf Kherkhachi [a], A. Attaf [a,*], H. Saidi [a], A. bouhdjar [a], H. Bendjdidi [a], Y. Benkhetta [a], R. Azizi [a], M.S. Aida [b]

[a] Physic Laboratory of Thin Films and Applications LPCMA, University of Biskra, Biskra, Algeria
[b] Laboratoire de Couches Minces et Interfaces Faculté des Sciences Université de Constantine, Constantine, Algeria

ARTICLE INFO

Article history:
Received 28 May 2015
Accepted 22 November 2015

Keywords:
Tin disulfide
Thin films
Molarity
Optical properties
Ultrasonic spray technique

ABSTRACT

SnS_2 thin film was deposited by spray ultrasonic technique, on pretreated glass substrates. The effect of SnS_2 concentration on different optical properties of SnS_2 thin films was investigated. X-ray diffraction study indicates that films have a hexagonal structure with preferential plan (0 0 1). SEM characterization technique shows that the morphology of these films is uniform, compact and granular. The results of (UV) spectroscopy in visible spectrum show that films deposited at 0.07 mol/l exhibits the largest transmittance. The optical energy band gap was found to be in the range 2.53–2.88 eV. The SnS_2 films showed average electrical resistivity of $4.62 \times 10^3\ \Omega$ cm.

1. Introduction

Currently there are investigations on novel materials for use in thin films solar cells other than the more extensively studied CdTe and $CuInSe_2$ [1]. But these materials suffer from environmental hazards and high cost of indium which are not beneficial for a mass production [2]. Among the different new materials available for solar cell fabrication, tin sulfide appears to be promising [1]. In the phase diagram of the Sn–S binary system, there are three stoichiometric stable compounds, with different tin to sulfur ratios: SnS, SnS_2 and Sn_2S_3 [3–5]. Tin disulfide (SnS_2) is a semiconductor with CdI_2 type structure [6]. It is a good light absorber (absorption coefficient of $10^4\ cm^{-1}$) with a varying band gap energy (0.8–2.88 eV) [7–9] composed with non-toxic and abundant raw materials [6]. These properties suggest that SnS_2 is a good potential candidate as a window material in thin film solar cells and optoelectronic device applications [10,11]. Moreover, SnS_2 can also be used as anode materials for lithium-ion battery due to its high theoretical capacities [12]. SnS_2 thin films can be prepared by several techniques such as molecular beam epitaxy [13], chemical vapor deposition [14], vacuum evaporation [15,16], dip coating [6,17] and chemical spray pyrolysis [9,18]. Among them, spray pyrolysis method is a cost effective technique to prepare tin disulfide thin film, since it is a low cost and can be used to deposit uniform coatings on large surface area [19]. The present study deals with the preparation and characterization of SnS_2 thin film deposited on the glass substrate at different molarity by ultrasonic spray method.

2. Experimental procedure

SnS_2 films used in the present work are prepared using a homemade ultrasonic spray deposition system (Fig. 1).

The sprayed solution is prepared from $SnCl_4$ ($5H_2O$) as a source of tin and CS $(NH_2)_2$ as a source of sulfide. In order to investigate the influence of $SnCl_4$ molarity (M_{Sn}) on films properties, we have prepared a solution with different molarities varying from 0.04 to 0.07 mol/l; however the thiourea molarity (M_S) was fixed to 0.1 mol/l.

The deposition conditions are summarized in Table 1.

The formation of SnS_2 phase from a solution can be schematized by the global reaction [17]:

$$SnCl_4 + 2(NH_2)_2CS + 2O_2 \rightarrow SnS_2 + 2NH_4Cl_2 + N_2 + 2CO_2$$

The structural studies were achieved using the diffractometer Bruker D8 ADVANCED conducted a Cu$K\alpha$ radiation source with a wavelength $\lambda = 1.5418$ Å length in the range 10–80°. The samples surface morphology was observed using a scanning electron microscope JEOL JSM 6301F model from which we deduced the thickness of the layers. A spectrophotometer UV–vis–NIR type "LAMBDA1050 PerkinElmer UV/vis/NIR Spectrometer" has been used in the range

* Corresponding author. Tel.: +213 773681758; fax: +213 33543190.
E-mail address: ab_attaf@univ-biskra.dz (A. Attaf).

http://dx.doi.org/10.1016/j.ijleo.2015.11.149
0030-4026/

Table 1
Parameters of deposit.

Molarity (mol/l) of $SnCl_4$ ($5H_2O$)	Amount of solution (ml)	Substrate temperature (°C)	Deposition time (min)	Distance Nozzle-substrate (cm)
0.04	30	350	10	4.5
0.05				
0.06				
0.07				

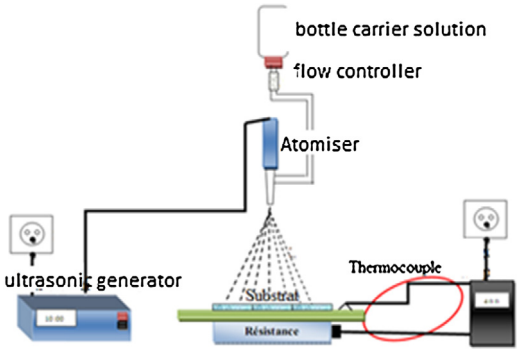

Fig. 1. Schematic diagram of the ultrasonic spray technique.

300–1500 nm for films optical characterization. The films resistivity measurement was achieved using four probes technique in dark and at ambient temperature.

3. Results and discussion

3.1. Structural study

The XRD diffraction spectra recorded in films prepared with various molarities are shown in Fig. 2.

The peak diffraction suggest that the obtained films are a SnS_2 with hexagonal structure (according to JCPDS card No 23-0677) with a preferential orientation in the plane (0 0 1) around the angle $2\theta = 15$, 02, this is consistent with the literature [20]. There is small difference for the peaks positions lattice parameters (a and c) between the experimental results and data. This may be caused by the defect in the cell of the crystal, which causes local changes in the lattice parameters. The results are shown in Table 2

The films crystallite size (D) are calculated from XRD patterns using the Scherrer's formula [21–25]

$$D = \frac{k\lambda}{\beta \times \cos\theta} \quad (1)$$

where k is a constant (0.94), β is the (full width half maximum) FWHM value, λ is the wavelength of CuK_α radiation source ($\lambda = 1.5418$ Å), and θ is the Bragg angle.

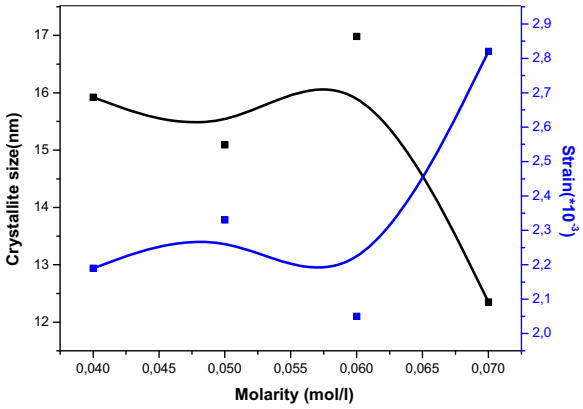

Fig. 3. Dependence of strain and crystallite size on molarity (M_{Sn}).

The strain (ε) developed in the film was estimated using the following relation [26]

$$\varepsilon = \frac{\beta \times \cos\theta}{4} \quad (2)$$

The variation of crystallite size and strain with molarity are showing in Fig. 3.

The crystallite size was varied in the range 12.35–16.98 nm. It was approximatively constant in the range of 0.04 to 0.06 mol/l, after the molarity of 0.06 mol/l, the grain size decreased. These values are comparable to those reported by Panda et al. [6] and Wei et al. [27]. The strain varies in the range of 2.19×10^{-3} to 2.82×10^{-3} with the variation of the molarity. The decrease in crystallite size in the thin layers of tin disulfide is due to the rise of the stress, this later is the results of internal strains [28]. Film prepared with 0.06 mol/l molarity has the minimum value of strain.

Knowing the crystallite size values one can estimate the dislocation density (δ), defined as the length of dislocation lines per unit volume of the crystal has been calculated by using the Williamson and Smallman's formula [29]:

$$\delta = \frac{1}{D^2} \quad (3)$$

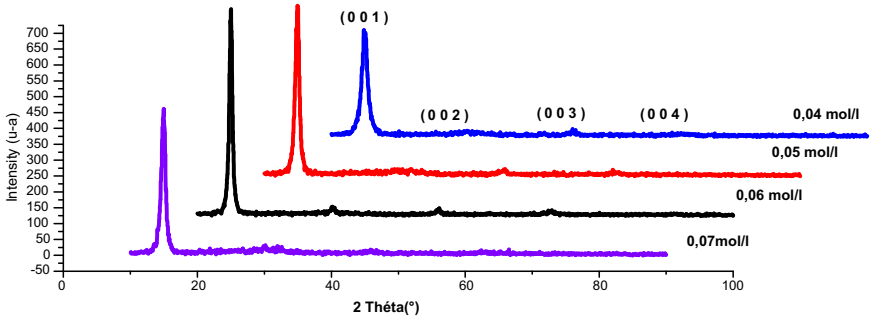

Fig. 2. XRD pattern of SnS_2 thin film sample with different molarity (M_{Sn}).

Table 2
Structural parameters of sprayed SnS_2 thin films.

SnS_2						JCPDS card reference No 23-0677	
Molarity (mol/l)	2θ (°)	*h k l* planes	Lattice parameters (Å)	Crystallite size (nm)	2θ (°)	Lattice parameters (Å)	
			a *c*			*a*	*c*
0.04	14.97	(0 0 1)	*a* = 3.628	15.92	15.02		
	30.06	(0 0 2)	*c* = 5.914				
	45.09	(0 0 3)					
	62.22	(0 0 4)				*a* = 3.648	
0.05	15.00	(0 0 1)	*a* = 3.623	15.09	30.26		
	30.06	(0 0 2)	*c* = 5.905				
	45.88	(0 0 3)					
	62.22	(0 0 4)				*c* = 5.899	
0.06	15.04	(0 0 1)	*a* = 3.613	16.98	46.1		
	30.24	(0 0 2)	*c* = 5.889				
	45.99	(0 0 3)					
	62.46	(0 0 4)					
0.07	15.08	(0 0 1)	*a* = 3.603	12.35	62.96		
	30.10	(0 0 2)	*c* = 5.873				
	45.90	(0 0 3)					

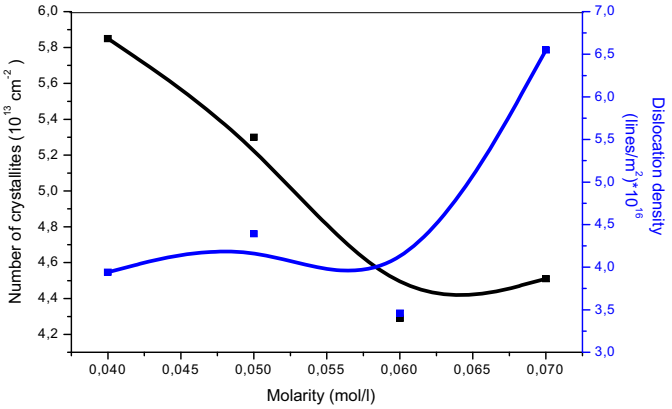

Fig. 4. The variation of number of crystallites and dislocation density with molarity of SnS_2 thin films.

Moreover, the number of crystallites per unit surface area can be calculated using the following formula [28].

$$n_c = \frac{e}{D^3} \quad (4)$$

where *e* is the film thickness which is about 0.85–2.35 μm and *D* is the crystallite size. The variations of the dislocation density and the number of crystallites are shown in Fig. 4. The number of crystallites decreased with increasing molarity in contrary to the dislocations.

3.2. Morphological study

The morphologies of the SnS_2 films were studied by SEM are shown in Fig. 5. The SEM micrographs show that the films have the same morphology. They are rough, dense, compact and uniform surface with less porosity and an arbitrarily distribution of the bubbles. This protuberances and bumps have been reported also by Messaoudi et al. in their study [30]. Fig. 6 is an enlargement of the SEM images (A, B, C and D) shown in Fig. 5. From these micrographs boiling phenomenon (explosion), probably due to the exo-diffusion of sulfide during film growth [31].

Fig. 7 shows the results of EDS, as can be seen tin and sulfide are present in a proportion variant around almost 35% and 65%, respectively (atomic percentage), according to the variation of the molarity these results are comparable to Amalraj et al. [18]. Other

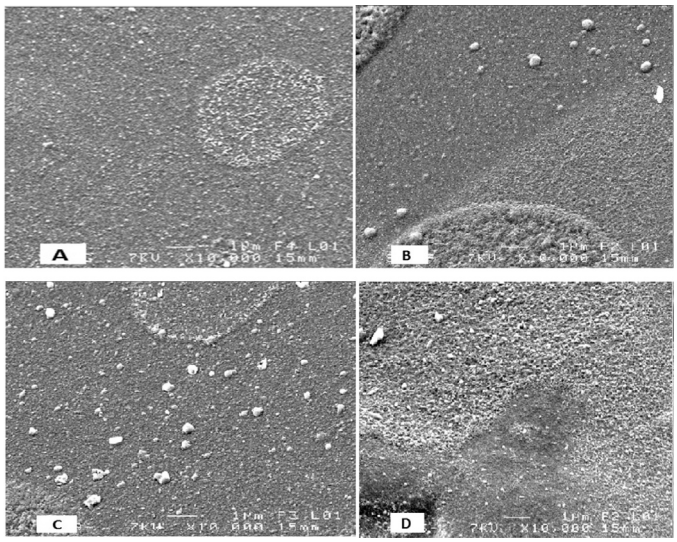

Fig. 5. The SEM micrograph of the SnS_2 thin films deposited at different molarities (A) 0 04 M, (B) 0.05 M, (C) 0.06 M, (D) 0.07 M.

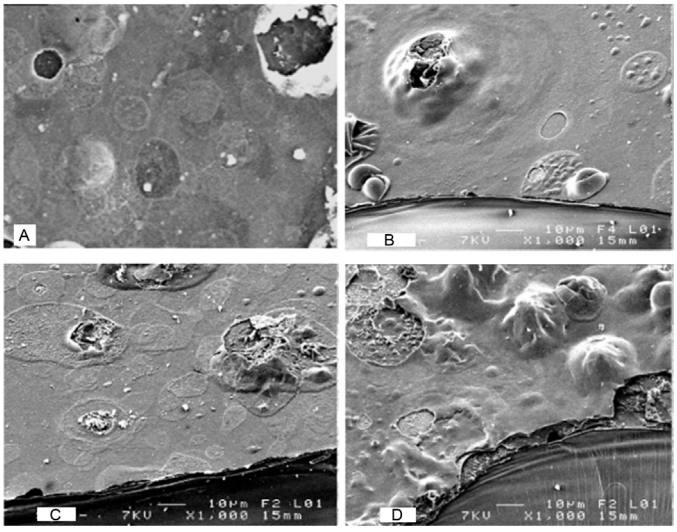

Fig. 6. Enlargement SEM images showing the phenomenon of explosion.

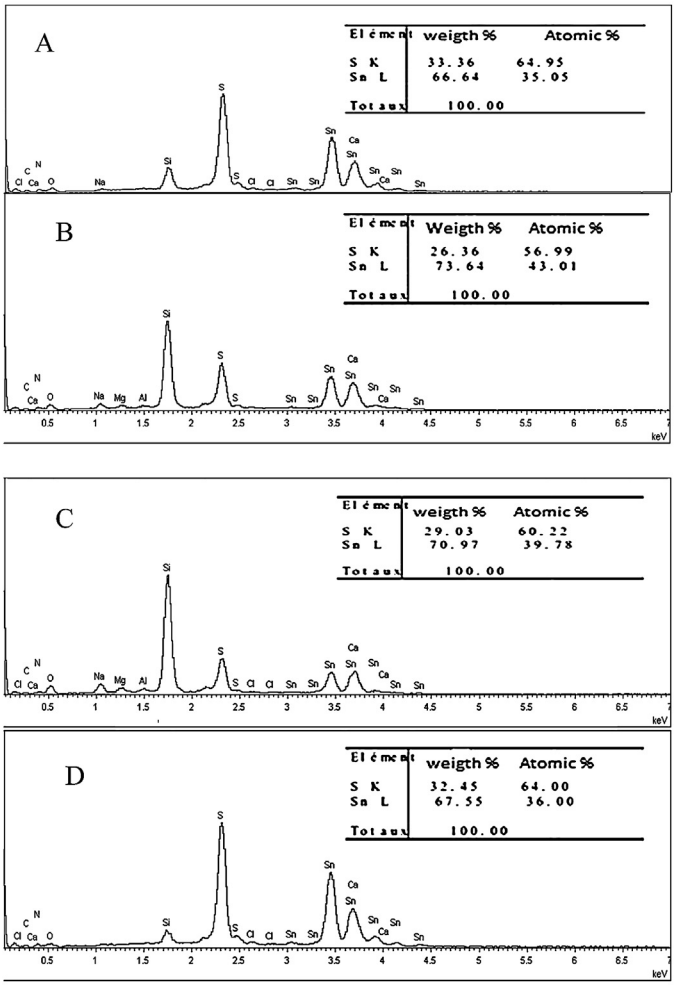

Fig. 7. EDS analysis results (A) 0.04 M, (B) 0.05 M, (C) 0.06 M, (D) 0.07 M.

elements with a small amount such as Si and oxygen are originating from the glass substrate, and Cl that comes from the starting solution.

3.3. Optical study

The optical transmittance with wavelength of tin disulfide films was measured in wavelength range of 300–800 nm. Fig. 8 shows the transmittance spectra of prepared SnS_2 films. The absence of interferences fringes in films transmittance spectra indicates that they

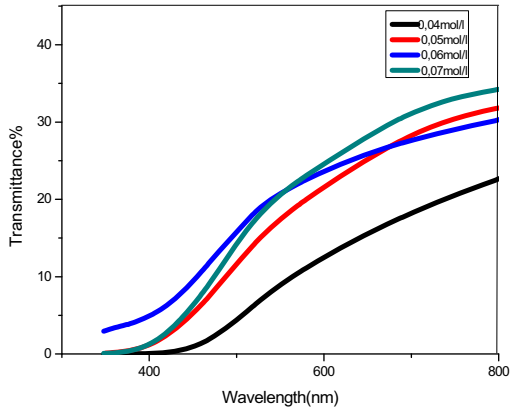

Fig. 8. Transmission curves for SnS_2 at different molarity (M_{Sn}).

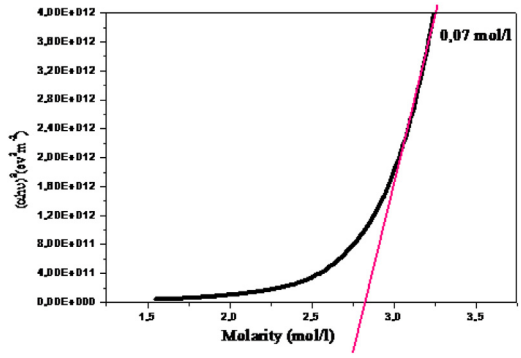

Fig. 9. The plot of $(\alpha h\upsilon)^2$ vs. $(h\upsilon)$ for SnS_2 film.

have a should rough surface morphology. The observed increase in the transmittance with increasing molarity is due to the reduction of films thickness.

The plot of $(\alpha h\upsilon)^2$ vs. $h\upsilon$ for SnS_2 thin film is shown in Fig. 9. The linear nature of the graph indicates the existence of direct transition. The band gap is determined by extrapolating the straight portion of the plot to the energy axis. The band gap (E_g) of our films, was determined from the transmittance spectra using the Tauc relation [32]:

$$(Ah\upsilon) = (h\upsilon - E_g)^n \tag{5}$$

where A is a constant, E_g is the optical band gap of the material and the exponent $n = 1/2$ stands for the allowed direct transitions. On the other hand, we have used the Urbach energy (E_u), which is related to the disorder in the film network, as it is expressed follow [33]:

$$A = A_0 \exp\left(\frac{h\upsilon}{E_u}\right) \tag{6}$$

where A_0 is a constant, $h\upsilon$ is the photon energy and E_u is the Urbach energy.

The optical gap decreases with increasing molarity and reaches a minimum at 0.06 mol/l after what it increase while the disorder varies inversely (Fig. 10). The values of optical gap are same with those obtained by precedent studies [34,35]. The variation of the optical gap and the variation of the crystallite sizes reveals that the gap has an opposite behavior regarding the crystallite variation and as already mentioned above due to the small crystallite size, we have a quantum restriction regime that may modify the electronic films properties. It is manifested by the appearance of discrete energy levels. So the crystallite size decreases the optical gap is widened. The widening of the gap is due to the reduction of the disorder in the film [32]. The disorder is characterized by the band tail width (valence and conduction). The optical gap is the

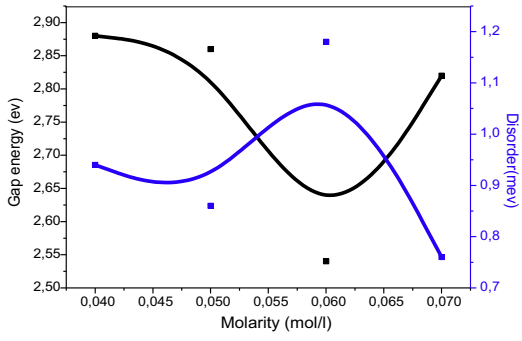

Fig. 10. Variation of band gap energy and disorder of SnS2 at different molarity (M_{Sn}).

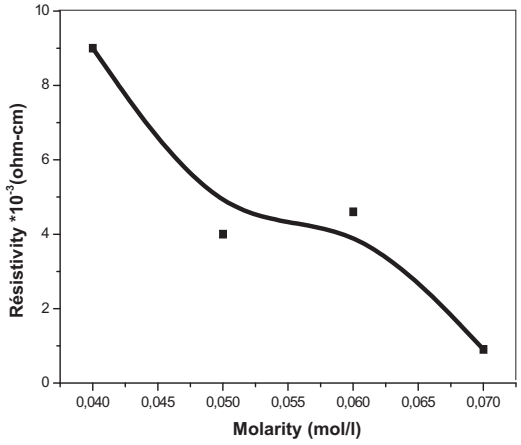

Fig. 11. Plot showing variation in Resistivity of the samples with molarity (M_{Sn}).

energy difference between the two band tail bands. Therefore, a disorder reduction is accompanied by an expansion of the optical gap [36].

3.4. Electrical study

The variation of films resistivity with molarity is depicted in Fig. 11. It is observed that resistivity decreases with increasing molarity. This is probably due to the increase in free carriers caused by the increase of the concentration of the solution. The room temperature resistivity is of the order of $10^3\ \Omega$ cm, which is in good agreement with the reported value [37,38]. Sajeesh et al. [2] studied the effect of molarity on electrical and structural properties of SnS films deposited by spray pyrolysis, and showed that the resistivity of SnS films was decreased with increasing of molarity (M_{sn}).

4. Conclusions

The spray ultrasonic technique has been successfully used to obtain SnS_2 films at various molarity. From the X-ray diffraction, we inferred that films have am hexagonal structure with preferential orientation (0 0 1). The SEM images indicate that film are dense with a rough surface morphology due to the sulfur exo-diffusion. EDS analysis confirm the elemental films composition with sulfur and tin in a proportion around almost 35% and 65% respectively. We conclude that the molarity variation alters the optical properties of SnS_2films. High absorbance was detected for the molarity 0.07 mol/l. The films had direct band gaps ranging from 2.53 to 2.88 eV depending on the crystallite size. The films resistivity varies from 9.04×10^3 to $0.92 \times 10^3\ \Omega$ cm.

References

[1] N. Koteswara Reddy, K.T. Ramakrishna Reddy, Growth of polycrystalline SnS films by spray pyrolysis, Thin Solid Films 325 (1998) 4–6.
[2] T.H. Sajeesh, A.R. Warrier, C. Sudha Kartha, K.P. Vijayakumar, Optimization of parameters of chemical spray pyrolysis technique to get n and p-type layers of SnS, Thin Solid Films 518 (2010) 4370–4374.
[3] L.A. Burton, A. Walsh, Phase Stability of the Earth-Abundant Tin Sulfides SnS, SnS_2, and Sn_2S_3, Phys Chem 116 (2012) 24262.
[4] X. Liu, H. Zhao, A. Kulka, A. Trenczek-Zajaç, Jingying. Xie, Ning. Chen, S. Konrad wierczek, Characterization of the physicochemical properties of novel SnS_2 with cubic structure and diamond-like Sn sublattice, Acta Materialia 82 (2015) 212–223.
[5] T. Chattopadhyay, A. Werner, H.G. Von Schnering, J. Pannetier, Temperature and pressure induced phase transition in IV-VI compounds, Revue de Physique Appliquee 19 (9) (1984) 807–813.
[6] S.K. Panda, A. Antonakos, E. Liarokapis, S. Bhattzcharya, S. Chaudhuri, Optical properties of nanocrystalline SnS_2 thin films, Mat. Res. Bull 42 (2007) 576.
[7] S. Acharya, O.N. Srivastava, Electronic behaviour of SnS_2 crystals, Phys. Status Solidi 65 (1981) 717–723.
[8] G. Domingo, R.S. Itoga, C.R. Kannewurf, Fundamental Optical Absorption in SnS_2 and $SnSe_2$, Phys. Rev 143 (1966) 536–541.
[9] B.B. Thangaraju, P. Kaliannan, Spray pyrolytic deposition and characterization of SnS and SnS_2 thin films Phys, D. Appl. Phys 33 (2000) 1054–1059.
[10] A. Sanchez-Juarez, A. Tiburcio-Silver, A. Ortiz, Fabrication of SnS_2/SnS heterojunction thin film diodes by plasma-enhanced chemical vapor deposition, Thin Solid Films 480 (2005) 452–456.
[11] K.T. Ramakrishna Reddy, G. Sreedevi, K. Ramya, Physical Properties of Nanocrystalline SnS_2 Layers Grown by Chemical Bath Deposition, Energy Procedia 15 (2012) 340–346.
[12] T. Momma, N. Shiraishi, A. Yoshizawa, Osaka, A. Gedanken, J. Zhu, L. Sominski, SnS_2 anode for rechargeable lithium battery, Power Sources 97 (2001) 198–200.
[13] R. Schlaf, N.R. Armstrong, B.A. Parkinson, C. Pettenkofer, W. Jaegermann, Van der Waals epitaxy of the layered semiconductors SnSe2 and SnS_2: morphology and growth modes, Surf .Sci 385 (1997) 1–14.
[14] R.D. Engelken, H.E. McCloud, C. Lee, M. Slayton, H. Ghoreishi, Low Temperature Chemical Precipitation and Vapor Deposition of Sn_xS Thin Films, Electrochem. Soc 134 (1987) 2696–2707.
[15] K. Kawano, R. Nakata, M. Sumita, Effects of substrate temperature on absorption edge and photocurrent in evaporated amorphous SnS_2 films, Phys. D Appl. Phys 22 (1989) 136.
[16] J. George, K.S. Joseph, Absorption edge measurements in tin disulphide thin films, Phys. D Appl. Phys 15 (1982) 1109.
[17] S.C. Ray, M.K. Karanjai, D. DasGupta, Structure and photoconductive properties of dip-deposited SnS and SnS_2 thin ®lms and their conversion to tin dioxide by annealing in air, Thin Solid Films 350 (1999) 72–78.
[18] L. Amalraj, C. Sanjeeviraja, M. Jayachandran, Spray pyrolysised tin disulphide thin film and characterization, Cryst Growth 234 (2002) 683–689.
[19] B. Thangaraju, P. Kaliannan, Polycrystalline Lead Tin Chalcogenide Thin Film Grown by Spray Pyrolysis Crystal Research and Technology 35 (2000) 71–75.
[20] C. Khelia, K. Boubaker, T. Ben Nasrallah, Mr. Amlouk, S. Belgacem, Morphological and thermal properties of SnS_2 crystals grown by spray pyrolysis technique, Alloys and Compounds 477 (2009) 461–467.
[21] L.I. Maissel, R. Glang, Handbook of Thin Film Technology, McGraw Hill, New York, 1970.
[22] B.E. Warren, X-ray diffraction, Dover, New York, 1990.
[23] K.T. Ramakrishna Reddy, N. Koteswara Reddy, R.W. Miles, Photovoltaic properties of SnS based solar cells, Solar Energy Materials & Solar Cells 90 (2006) 3041–3046.
[24] M. Devika, K.T.R. Reddy, N.K. Reddy, K. Ramesh, E.S.R. Gopal, K.R. Gunasekhar, Microstructure dependent physical properties of evaporated tin sulfide films, Appl.Phys 100 (2006) 023518.
[25] Z. Qiao, R. Latz, D. Mergl, Thickness dependence of In2O3:Sn film gowth, Thin Solid Films 466 (2004) 250–258.
[26] K.L. Chopra, Thin Film Phenomena, McGraw-Hill, New York, 1969, pp. 270.
[27] R. Wei, T. Zhou, J. Hu, J. Li, Glutatione modified ultrathin SnS_2 nanosheets with highly photocatalytic activity for wastewater treatment, Materials Research Express 1 (2014) 025018.
[28] B.G. Jeyaprakash, R. Ashok kumar, K. Kesavan, A. Amalarani, Structural and optical characterization of spray deposited sns thin film, American Science 6 (2010) 3.
[29] G.B. Williamson, R.C. Smallman III, Dislocation densities in some annealed and cold-worked metals from measurements on the X-ray debye-scherrer spectrum, Philosophical Magazine 1 (1956) 34–46.
[30] M. Messaoudi, M.S. Aida, N. Attaf, T. Bezzi, Deposition of tin (II) sulfide thin films by ultrasonic spray pyrolysis: Evidence of sulfur exo-diffusion, J. Bougdira, G. Medjahdi, Materials Science in Semiconductor Processing 17 (2014) 38–42.
[31] M. Calixto-Rodriguez, H. Martinez, A. Sanchez-Juarez, A. Campos-Alvarez, M.E. Tiburcio-Silver, Calixto, Structural, optical, and electrical properties of tin sulfide thin films grown by spray pyrolysis, Thin Solid Films 517 (2009) 2497–2499.
[32] J.I. Pankove, Optical processes in semiconductors, Dover, New York, 1975.
[33] S. Benramache, B. Benhaoua, O. Belahssen, The crystalline structure, conductivity and optical properties of Co-doped ZnO thin films, Optik 125 (2014) 5864–5868.
[34] N.G. Deshpande, A.A. Sagade, Y.G. Gudage, C.D. Lokhande, Growth and characterization of tin disulfide (SnS_2) thin film deposited by successive ionic layer adsorption and reaction (SILAR) technique, Alloy Compd 436 (2007) 421–426.
[35] O.V. Parasyuk, I.D. Olekseyuk, L.V. Piskach, S.V. Volkov, V.I. Pekhnyo, Phase relations in the Ag2S–CdS–SnS_2 system and the crystal structure of the compounds, Alloys Compd 399 (2005) 173–177.
[36] W. Daranfed, M.S. Aida, A. Hafdallah, H. Lekiket, Substrate temperature influence on ZnS thin films prepared by ultrasonic spray, Thin Solid Films 518 (2009) 1082–1084.
[37] C.D. Lokhande, A chemical method for tin disulphide thin film deposition, Phys D Appl Phys 23 (1990) 703.
[38] B.R. Sankapal, R.S. Mane, C.D. Lokhande, Successive ionic layer adsorption and reaction (SILAR) method for the deposition of large area (~10 cm2) tin disulfide (SnS_2) thin films, Materials Research Bulletin 35 (2000) 2027–2035.